Journal of Materials Chemistry A

ROYAL SOCIETY OF CHEMISTRY

REVIEW

View Article Online
View Journal | View Issue

Cite this: J. Mater. Chem. A, 2021, 9, 7407

Designing positive electrodes with high energy density for lithium-ion batteries

Masashi Okubo, [ab] Seongjae Ko,[a] Debasmita Dwibedi[a] and Atsuo Yamada *[ab]

The development of efficient electrochemical energy storage devices is key to foster the global market for sustainable technologies, such as electric vehicles and smart grids. However, the energy density of state-of-the-art lithium-ion batteries is not yet sufficient for their rapid deployment due to the performance limitations of positive-electrode materials. The development of large-capacity or high-voltage positive-electrode materials has attracted significant research attention; however, their use in commercial lithium-ion batteries remains a challenge from the viewpoint of cycle life, safety, and cost. In this review, after summarizing the limitation issues associated with large-capacity/high-voltage positive electrodes and already attempted technical solutions, a machine-learning technique is applied to analyze the reported dataset to hierarchize various technical solutions by their effectiveness in improving performance. The proposed study highlights the importance of integrating systematic experimental data collection with modern data analysis techniques for rational development of large-capacity/high-voltage positive electrodes. The scope is extended to important technical issues with other cell components, such as electrolytes and additives, binders, conductive carbon, current collectors, and impurity control for total optimization.

Received 21st October 2020
Accepted 29th December 2020

DOI: 10.1039/d0ta10252k

rsc.li/materials-a

1. Introduction

Lithium-ion batteries (LIBs) have been widely used in consumer electronics, which has resulted in the rapid growth of the LIB market in the 2000s. In the 2010s, the deployment of electric vehicles (EVs), which was accelerated by favorable governmental policies, reached a global stock of 5 million EVs in 2018, which further increased the LIB production to greater than 100 GW h per year.[1] As the EV stock is predicted to reach 250 million in 2030, the automotive industry is eagerly seeking LIB technology that realizes long drive distances, low cost, and a robust cycle life for EVs, bearing in mind the second use of LIBs as stationary energy storage.

The EV drive distance is linked to the energy density of the LIB. While the existing LIB cells possess an energy density of approximately 200–250 W h kg^{-1}, the national targets of most leading countries are greater than 300 W h kg^{-1} for EV market growth.[2] However, LIBs comprising conventional positive and negative electrodes have already approached their performance limits, and they can hardly reach these national targets due to the relatively moderate capacities/voltages of the electrodes.[3] Battery engineers are attempting to exploit the large-capacity or high-voltage positive electrodes or large-capacity negative electrodes for increasing the energy density of LIBs. Indeed, the capacity of negative electrodes in the recent commercial LIBs has been successfully increased using silicon or silicon oxides as electrode additives.[4]

In contrast, despite decades of intensive research, the use of large-capacity or high-voltage positive electrodes remains challenging. Positive-electrode materials are typically classified into three categories, *i.e.* layered oxides ($LiTMO_2$, TM: transition metal), spinel oxides ($LiTM_2O_4$), and polyanionic compounds ($Li_xTM_y(XO_n)_z$, X: P, S, B, Si, *etc.*).[5–10] For example, the layered oxide, $LiCoO_2$, delivers a specific capacity of approximately 140–150 mA h g^{-1} at an average voltage of 3.9 V *vs.* Li/Li^+ when cycled with an upper cut-off voltage of 4.2 V *vs.* Li/Li^+.[5] Meanwhile, $LiMn_2O_4$ is a conventional spinel oxide that delivers a specific capacity of approximately 120–130 mA h g^{-1} at an average voltage of 4.0 V *vs.* Li/Li^+ (upper cut-off voltage of 4.2 V *vs.* Li/Li^+).[6] Finally, $LiFePO_4$ is a typical polyanionic compound that can deliver a specific capacity of approximately 160–170 mA h g^{-1} at an average voltage of 3.4 V *vs.* Li/Li^+.[7,11] Although all these electrode materials have been used in commercial LIBs, their available specific capacity is far below the requirement of the EV industry (Fig. 1a), which has devoted considerable efforts in developing large-capacity/high-voltage positive electrodes.

Nickel-rich layered oxides are the most promising large-capacity positive electrode, as they deliver a specific capacity greater than 200 mA h g^{-1} (Fig. 1b).[12–14] Lithium-rich layered oxides are another important family of layered oxides with

[a]Department of Chemical System Engineering, School of Engineering, The University of Tokyo, Hongo 7-3-1, Bunkyo-ku, Tokyo 113-8656, Japan. E-mail: yamada@chemsys.t.u-tokyo.ac.jp

[b]Elemental Strategy Initiative for Catalysts & Batteries (ESICB), Kyoto University, Nishikyo-ku, Kyoto 615-8510, Japan

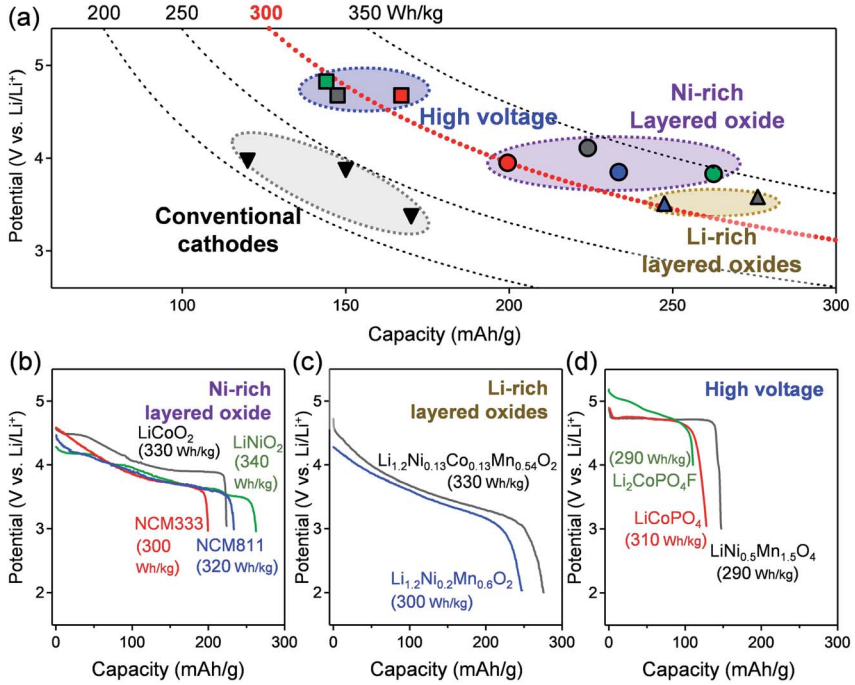

Fig. 1 (a) Plot of the capacities and averaged voltages of positive-electrode materials during the first discharge. The performance metrics of conventional materials ($LiMn_2O_4$, $LiCoO_2$, and $LiFePO_4$) are also plotted for comparison. Dotted lines are the expected energy densities of lithium-ion batteries (negative electrode: graphite). Discharge curves of (b) nickel-rich layered oxides ($LiNiO_2$ and NCM811 ($LiNi_{0.8}Co_{0.1}Mn_{0.1}O_2$)) and conventional layered oxides for comparison ($LiCoO_2$ and NCM333 ($LiNi_{1/3}Co_{1/3}Mn_{1/3}O_2$)), (c) lithium-rich layered oxides ($Li_{1.2}Ni_{0.13}Co_{0.13}Mn_{0.54}O_2$ and $Li_{1.2}Ni_{0.2}Mn_{0.6}O_2$), and (d) high-voltage spinel oxide ($LiNi_{0.5}Mn_{1.5}O_4$) and polyanionic compounds ($LiCoPO_4$ and Li_2CoPO_4F). The expected energy density of each cathode material (negative electrode: graphite) is noted for reference.

a large specific capacity of >250 mA h g^{-1} (Fig. 1c).[15–17] High-voltage positive-electrode materials, such as spinel oxides and polyanionic compounds, operating at an average voltage of >4.7 V *vs.* Li/Li^+ have also been studied intensively (Fig. 1d).[18–21] Theoretically, their effective adoption in LIBs will result in energy densities greater than 300 W h kg^{-1} (Fig. 1a).

However, even when we intuitively consider the intercalation chemistry of a positive-electrode reaction as $n\mathrm{Li}^+ + n\mathrm{e}^- + \mathrm{A} \rightarrow \mathrm{Li}_n\mathrm{A}$ (where A is host), a large capacity corresponds to a large n, whereas a high voltage corresponds to a low lithium chemical potential (μ_{Li}) of the host. For both the cases, electrode reactions are associated with a large standard reaction Gibbs energy of the electrode material ($|\Delta_r G^\circ| = \Sigma_n|\mu_{\mathrm{Li}}|$), which generally leads to the formation of unstable (de)lithiated phases and/or large change in the unit cell volume during (de)lithiation; this, in turn, rapidly degrades the reversible capacity upon cycling. Further, a large difference between the standard reaction Gibbs energies of positive and negative electrodes, which are separated by a flammable organic electrolyte, can trigger thermal runaway and fire explosion accidents. When using large-capacity/high-voltage positive electrodes, another important requirement is an electrolyte with high stability against oxidation. As the EV industry must achieve a high energy density and should simultaneously reduce the costs, the potential candidates for chemical components of positive-electrode materials, electrolytes, and binders are severely limited. For example, reducing the content of expensive and scarce cobalt is a primary requirement, whereas a long calendar life should also be obtained. Under these multiple severe restrictions, only an atomistic understanding of the degradation mechanisms of each component and their interfaces/interphases can enable the rational electrode developments and improvements.

Although several complementary reviews have summarized the practical limitations associated with some positive-electrode materials and their technical solutions,[22–34] in this review, we aim to establish a multiscale (micro/meso/macroscopic) overview of large-capacity/high-voltage positive-electrode materials. A machine-learning technique is applied to analyse and obtain the most efficient technical approaches towards higher energy density with minimal trade-offs.

2. Origins of large capacity/high voltage

Let us consider an electrode reaction:

$$n\mathrm{Li}^+ + n\mathrm{e}^- + \mathrm{A} \rightarrow \mathrm{Li}_n\mathrm{A},$$

where A is the host material. The specific capacity (Q) under an operating voltage window, ΔE, is expressed as follows:

$$Q = \frac{nF}{M} = \frac{F}{M}\int_{\varepsilon_F - F\Delta E + \Delta\mu_{\mathrm{Li}^+}}^{\varepsilon_F} D(\varepsilon)\mathrm{d}\varepsilon$$

where F is the Faraday constant, M is the molecular weight of A, ε_F is the Fermi energy of A, $\Delta\mu_{Li^+}$ is the difference between the lithium-ion chemical potentials of A and Li_nA, and $D(\varepsilon)$ is the density of states of A, respectively. The average reaction voltage, E_{av} [*vs.* Li/Li^+], is given as follows:

$$E_{av} = -\frac{1}{nF}\int_0^n \{\mu_{Li^+}(n') + \mu_{e^-}(n')\}dn'$$

where μ_{Li^+} and μ_{e^-} are the lithium-ion and electron chemical potentials of Li_nA, respectively. According to these expressions, using electrode materials with a large $D(\varepsilon)$ for $\varepsilon_F > \varepsilon > \varepsilon_F - F\Delta E + \Delta\mu_{Li^+}$) achieves a large capacity, whereas those with low μ_{Li^+} or low μ_{e^-} achieves a high voltage.

One of the most promising positive electrode materials for achieving high energy density is a nickel-rich layered oxide, *i.e.* $LiNi_xTM_{1-x}O_2$ (TM: Mn, Co).[12,13,35–37] For example, $LiNi_{0.8}Co_{0.1}Mn_{0.1}O_2$ (NCM811) typically delivers a large specific capacity of approximately 200 mA h g^{-1} at an average voltage of 3.8 V *vs.* Li/Li^+ (Fig. 1b; operation voltage: 3.0–4.5 V *vs.* Li/Li^+).[33,34] In general, increasing the nickel content by replacing cobalt increases the specific capacity (*e.g.* $LiCoO_2$ *vs.* $LiNiO_2$, $LiNi_{1/3}Co_{1/3}Mn_{1/3}O_2$ (NCM333) *vs.* NCM811) (Fig. 1b).[5,12,38–41] As the frontier energy level of Ni e_g–O 2p antibonding bands is higher (*i.e.* higher μ_{e^-}) than that of Co t_{2g} nonbonding bands, the reaction voltage of $LiNiO_2$ (3.8 V *vs.* Li/Li^+) is lower than that of $LiCoO_2$ (4.1 V *vs.* Li/Li^+) (Fig. 1b). Consequently, nickel-rich layered oxides exhibit a large amount of (de)lithiation, even under a low upper cut-off voltage (larger integrated $D(\varepsilon)$ for $\varepsilon_F > \varepsilon > \varepsilon_F - F\Delta E + \Delta\mu_{Li^+}$). Meanwhile, replacing manganese with nickel (altering Mn^{3+} to $Mn^{4+}{}_{0.5}Ni^{2+}{}_{0.5}$, then to Ni^{3+}) decreases the number of strong Jahn–Teller Mn^{3+} ions,[42,43] thereby suppressing large structural distortions and enabling a large capacity with somewhat better reversibility.

To confirm the influence of the nickel content on the specific capacity, we applied a machine-learning technique to a data-set assembled from the reported capacities of nickel-rich layered oxides.[38,41,44–112] The supervised learning of the reported discharge capacities during the first cycle was conducted using a random forest regression with five simple features, *i.e.* Ni, Co, and Mn contents, upper cut-off voltage, and charge/discharge C rate. Fig. 2a compares the predicted and actual discharge capacities (R^2 = 0.82 and 0.70 for the training and test data, respectively), suggesting the reasonable generalization performance of the model, even with only five simple features. As shown in Fig. 2b, except for the extrinsic experimental conditions (upper cut-off voltage and charge/discharge C rate), Ni content is the most important feature for explaining the trend in the specific capacity of nickel-rich layered oxides (Fig. 3a), which supports the above discussion. Conversely, the Co content is a negative explanatory variable for the discharge capacity.

Another important class of layered oxides capable of a large storage capacity is lithium-rich layered oxides, $Li_{1+x}TM_{1-x}O_2$.[15–17,25–27,113] For example, $Li_{1.2}Ni_{0.13}Co_{0.13}Mn_{0.54}O_2$ and $Li_{1.2}Ni_{0.2}Mn_{0.6}O_2$ deliver specific capacities greater than 250 mA h g^{-1} (Fig. 1c).[114,115] As the transition metals are partially replaced by lithium ions, the coordination

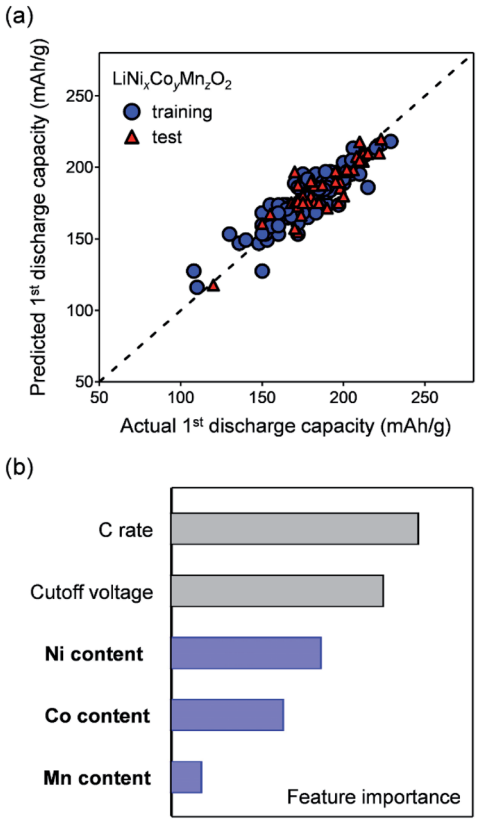

Fig. 2 (a) Predicted *versus* actual discharge capacities of nickel-rich layered oxides during the first cycle. (b) Importance of each of the five features (Ni, Co, and Mn contents, upper cut-off voltage, and charge–discharge C-rate).

environment of oxide ions involves a specific axis of Li–O–Li, along which an oxygen 2p orbital remains nonbonding near ε_F to contribute to the charge compensation for (de)lithiation (additional $D(\varepsilon)$, Fig. 3b).[116–118] Although the chemical state of oxidized oxygen after delithiation has long been debated,[119–124] accumulative redox reactions by both the transition metals (cationic redox) and oxide ions (anionic redox or oxygen redox) provide large specific capacities.[125] Unlike nickel-rich layered oxides, a machine-learning technique applied to the reported capacities of lithium-rich layered oxides with simple features (such as Li, Mn, Co, and Ni contents, upper cut-off voltage, or charge/discharge C rate) could not provide a reasonable prediction model with good generalization performance. Presumably, other complicated factors, such as particle morphology, carbon additive, electrolyte composition, and initial activation process, which were not considered in the supervised learning, could influence the capacities of the lithium-rich layered oxides.

$LiNi_{0.5}Mn_{1.5}O_4$ is a representative high-voltage spinel oxide for positive electrodes, wherein Mn^{3+} in $LiMn_2O_4$ is replaced by Ni ($Mn^{3+} \rightarrow Mn_{0.5}{}^{4+}Ni_{0.5}{}^{2+}$), and the two-electron redox reaction of $Ni^{4+}/Ni^{3+}/Ni^{2+}$ occurs.[18,126,127] Unstable Jahn–Teller Ni^{3+} increases the reaction voltage of Ni^{3+}/Ni^{2+}, while lowering the reaction voltage of Ni^{4+}/Ni^{3+}, thereby leading to a continuous potential profile for the two-electron redox capacity. Lithium

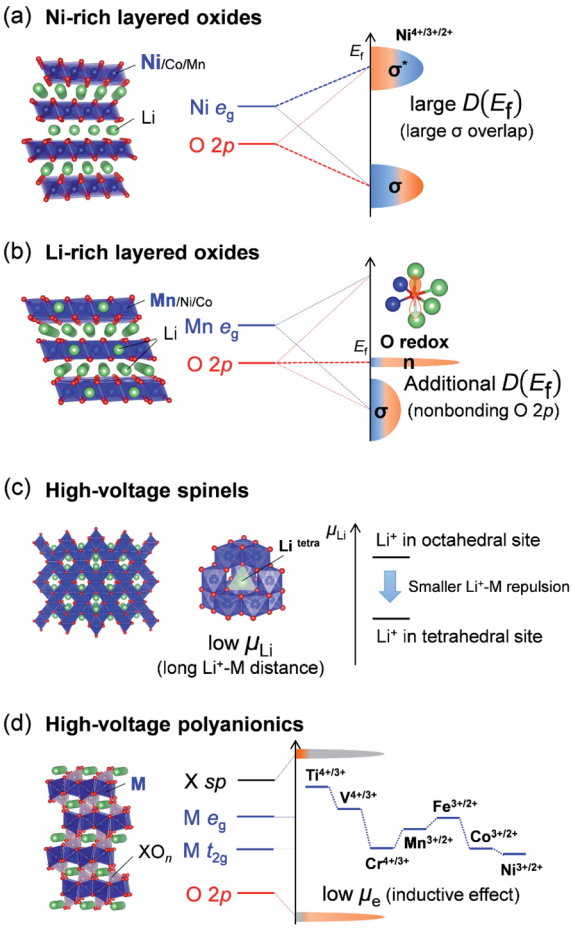

Fig. 3 Origins of the high performance of (a) nickel-rich layered oxides, (b) lithium-rich layered oxides, (c) high-voltage spinels, and (d) high-voltage polyanionic compounds.

ions occupy tetrahedral 8a sites, which are located away from the transition metals in octahedral 16d sites. The coulombic repulsion between lithium ions and transition metals is lower than that of layered oxides (where lithium ions occupy octahedral 3*a* sites near the transition metals in octahedral 3*b* sites), which in turn yields a lower μ_{Li^+}, resulting in a high voltage of approximately 4.8 V *vs.* Li/Li^+ (Fig. 3c). Indeed, similar high reaction voltages have been reported for other spinel oxides $LiTM_{0.5}Mn_{1.5}O_4$ (TM: Co, Cr) with little dependence on TM.[127–129]

Polyanionic compounds such as $LiCoPO_4$ are another family of high-voltage positive-electrode materials.[20,130] Transition metals in polyanionic compounds are mainly coordinated by the oxygen atoms of oxyanions (XO_n^{m-}, X: P, S, B, and Si), wherein the oxygen atom predominantly donates the electrons to X atom (a covalent X–O bond), resulting in a highly ionic TM–O bond. The energy levels of TM–O antibonding states composed of predominantly TM 3d orbitals under ionic coordination environments (small TM–O bonding–antibonding splitting) are much lower (*i.e.* lower μ_{e^-}) than those under more covalent coordination environments, such as those of transition-metal oxides.[10,131] In addition, the large interstitial spaces for lithium ions decrease lithium-ion chemical potential (low μ_{Li^+}). Owing to these combined effects, polyanionic compounds generally exhibit high reaction voltages (Fig. 3d). In particular, as the redox couple of Co^{3+}/Co^{2+} has a significantly low μ_{e^-} owing to the electronic configuration of high-spin Co^{3+} ($t_{2g}^4e_g^2$), $LiCoPO_4$ operates at a high average voltage of approximately 4.8 V *vs.* Li/Li^+. The redox couples of Ni^{3+}/Ni^{2+} (stable Ni^{2+} ($t_{2g}^6e_g^2$)) and Cr^{4+}/Cr^{3+} (stable Cr^{3+} (t_{2g}^3)) are also expected to have low μ_{e^-}, leading to high reaction voltages.[132–137] In addition, incorporating a highly ionic fluoride ion into the coordination environment of transition metals (*e.g.* Li_2CoPO_4F) further lowers μ_{e^-} and raises the reaction voltage.[138–143]

3. Oxidation stability of electrolytes

The oxidation stability of electrolytes is crucial for the stable operation of large-capacity/high-voltage positive electrodes.[144] Fig. 4 shows systematic linear sweep voltammetry results of various electrolytes with an aluminium current collector, conductive carbon (acetylene black), oxide electrode ($LiMn_2O_4$), and polyanionic electrode ($LiCoPO_4$).

The first requisite for electrolytes is to suppress aluminium corrosion at high voltages. Imide anions (such as bis(fluorosulfonyl)imide (FSI^-) and bis(trifluoromethanesulfonyl) imide ($TFSI^-$)) severely corrode aluminium below 4.2 V *vs.* Li/Li^+ because of the formation of soluble $Al(FSI)_3$ and $Al(TFSI)_3$ complexes (Fig. 4a).[145,146] Although employing a high salt concentration can hinder the dissolution of these complexes to suppress aluminium corrosion,[147] imide anions may not be a primary option for large-capacity/high-voltage electrodes. In contrast, the BF_4^- anion does not exhibit anodic current flow below 5.3 V *vs.* Li/Li^+,[148] which is compatible with large-capacity positive electrodes. As the PF_6^- anion possesses the best oxidation stability up to 6.0 V *vs.* Li/Li^+,[148,149] it is the best anion for large-capacity/high-voltage positive-electrode materials. For both BF_4^- and PF_6^- anions, insoluble AlF_3 forms, which passivates the current collector surface.[150]

The second requisite is to suppress the parasitic oxidation of the electrolyte components. Conductive carbon additives in large-capacity/high-voltage positive electrodes possess a large specific surface area, which generally results in nontrivial parasitic oxidation. Fig. 4b shows that a conductive carbon (acetylene black) electrode exhibits a small anodic current flow at 4.1 V *vs.* Li/Li^+ with conventional electrolytes. This current flow is attributed to the oxidation of electrolyte solvents rather than that of the conductive carbon,[151–153] because the current does not flow with an oxidation-durable fluorinated solvent, *i.e.* fluoroethylene carbonate (FEC). However, the further oxidation of carbonate electrolytes is suppressed up to 4.7 V *vs.* Li/Li^+, suggesting the formation of a cathode-electrolyte interphase (CEI) at approximately 4.1 V *vs.* Li/Li^+.[155] In contrast, continuous anodic current above 4.1 V *vs.* Li/Li^+ for ether electrolytes, such as dimethyl ether (DME), indicates their incompatibility with large-capacity/high-voltage electrodes.[154] As identical results were obtained for an oxide electrode ($LiMn_2O_4$) containing a carbon additive (Fig. 4c), the active site for CEI formation should be the electrophilic surface of the conductive carbon,

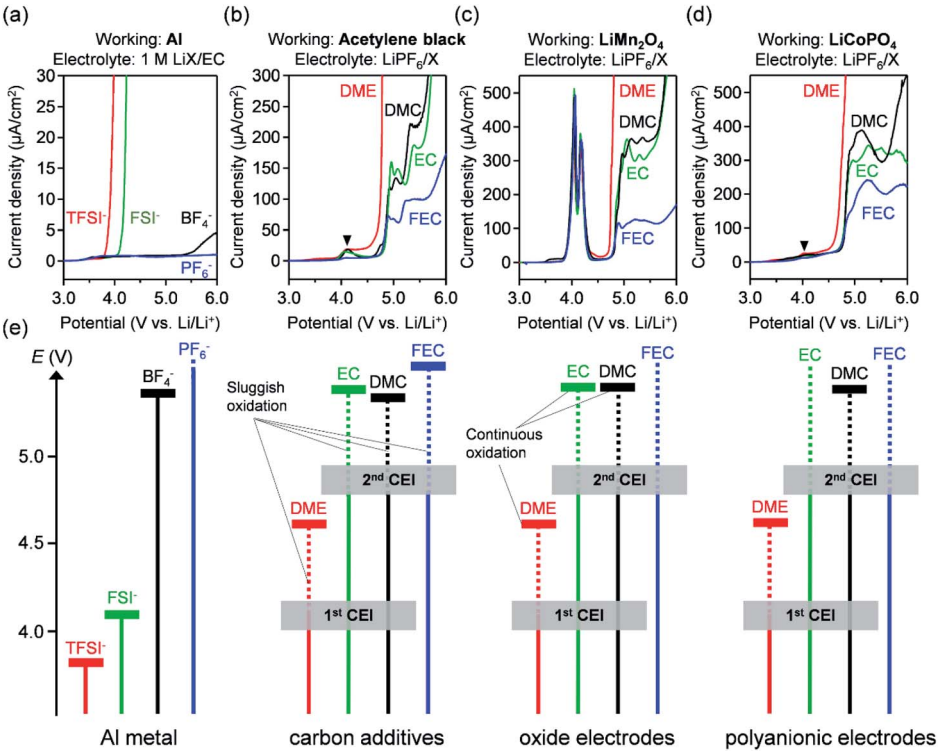

Fig. 4 Anodic stability of electrolytes. Linear sweep voltammetry at 30 °C of (a) an aluminum current collector with 1 M LiX/EC (X: FSI^-, $TFSI^-$, BF_4^-, and PF_6^-), (b) conductive carbon (acetylene black) electrode, (c) $LiMn_2O_4$ electrode, and (d) $LiCoPO_4$ electrode with $LiPF_6$/X (X: DME, DMC, EC, and FEC). The concentration of the electrolytes is 1.0 M except for DME (0.5 M). (e) Summary of the anodic stabilities of 1 M $LiPF_6$ electrolytes (solvents: linear ether (DME)), linear carbonate (DMC), cyclic carbonate (EC), and fluorinated cyclic carbonate (FEC).

which abstracts the electrons from solvent molecules. In particular, the electron abstraction of carbonates generates the radical cations of alkyl carbonates (R^+–$OCOO^\bullet$; R = alkyl group), forming CEIs *via* their polymerization.[150] Owing to this protective CEI formation, carbonate electrolytes are compatible with large-capacity electrodes (typically up to 4.4 and 4.7 V *vs.* Li/Li^+ for nickel-rich layered oxides and lithium-rich layered oxides, respectively). Indeed, the major electrolytes for large-capacity electrodes are 1.0–1.2 M $LiPF_6$ in a mixture of cyclic and linear carbonates.

To stably operate high-voltage electrodes, an electrolyte should be electrochemically stable above 4.8 V *vs.* Li/Li^+. However, even relatively oxidation-resistant linear/cyclic carbonates exhibit sluggish but continuous oxidation above 4.7 V *vs.* Li/Li^+ (Fig. 4d). As fluorinated carbonates, such as FEC, slightly suppress the anodic oxidation, perhaps owing to their low highest occupied molecular orbital (HOMO) levels and/or the formation of fluorine-rich CEI, the fluorination of electrolyte solvents can be a practical option for improving the reversibility and capacity retention of high-voltage electrodes.[88,156] For example, an electrolyte consisting solely of fluorinated solvents (FEC/methyl(2,2,2-trifluoroethyl)carbonate (FEMC)/1,1,2,2-tetrafluoroethyl-2′,2′,2′-trifluoroethyl ether (HFE)) was proposed for high-voltage electrodes.[88] However, achieving an intrinsic oxidation stability above 4.7 V *vs.* Li/Li^+ is still a major challenge (Fig. 5a).

4. Issues and technical solutions

4.1. Intrinsic degradation

Cations (lithium and transition-metal ions) in a positive-electrode material occupy interstitial (*e.g.* octahedral/tetrahedral) sites in an array of anions (oxide ions or oxyanions), and lithium ions are deintercalated to generate lithium-ion vacancies V'_{Li} (Kröger–Vink notation) upon charge as follows:

$$Li^{\times}_{Li}TM^{\times}_{oct} \rightarrow V'_{Li}TM^{\bullet}_{oct} + Li^+ + e^-,$$

where attractive forces between V'_{Li} and $TM^{\bullet}_{oct}$ tend to drive the migration of TM to lithium-ion vacancies (cation migration).[157–160] A large capacity generates a large amount of V'_{Li} upon charging, whereas high voltage forms vacant sites with low μ_{Li^+} (*i.e.* an unstable vacancy), both of which accelerate the migration of TM. Because TM ions at lithium-ion sites hinder lithium-ion diffusion, cation migration is a common atomistic degradation mechanism in most positive electrode materials (Fig. 5a).

From a meso/macroscopic viewpoint, layered oxides comprise alternating stackings of Li^+ and TMO_2 slabs. Although a pristine layered structure is stabilized by Li^+–O^{2-} coulombic attractions, significantly weaker van der Waals force between the TMO_2 slabs becomes dominant in deeply delithiated (charged) states, thereby triggering a damaging phase transition (*e.g.* hexagonal 2 phase (H2) → hexagonal 3 phase (H3)), during

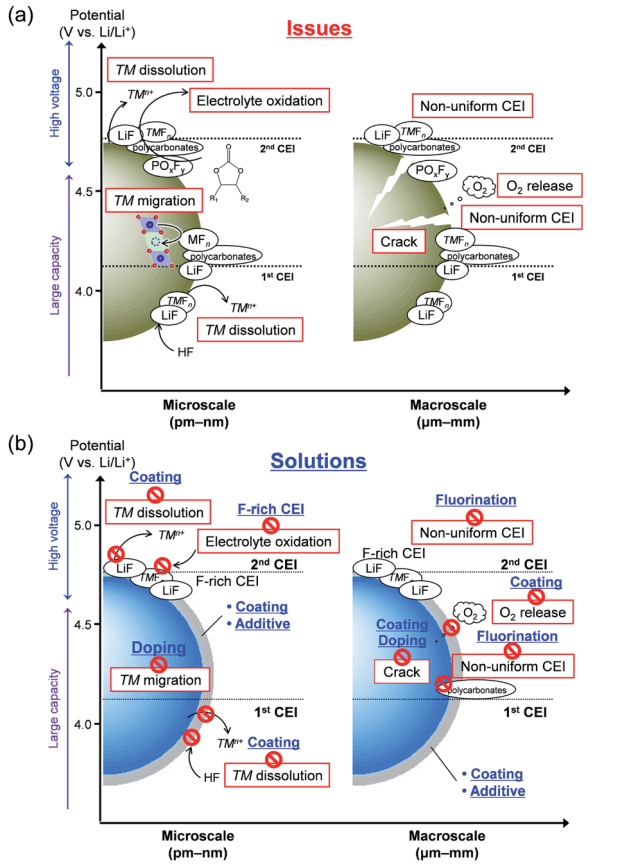

Fig. 5 (a) Issues with large-capacity/high-voltage positive electrodes, and (b) solutions to these issues.

which the unit cell volume considerably changes by over 7%.[161] This large volume change, along with gliding of the TMO_2 slabs upon deep charging, can delaminate the TMO_2 slabs and crack, fracture, and/or pulverization $LiTMO_2$ particles, which severely degrades the electrode composite (Fig. 5a).[157,161]

For lithium-rich layered oxides, a large capacity is achieved by the additional redox reaction of oxide ions. An oxidized oxide ion has an unstable electronic configuration ($2p^5$) and may easily dimerize, for instance, to form a peroxide-like ion (O_2^{2-}).[119,122,162] Such dimerized ions should be further oxidized to O_2 at a high voltage, resulting in a large amount of oxygen vacancies, which predominantly form on the particle surface. In turn, these vacancies cause the formation of cation-densified phases that are electrochemically inactive (Fig. 5a).[116,123,163]

High-voltage spinel oxides possess a three-dimensional framework of TM_2O_4, through which lithium ions diffuse three-dimensionally. Because this framework is rigid, the unit cell volume changes by less than 6% during delithiation,[164,165] limiting crack formation. Therefore, the migration of TM is the major intrinsic mode of degradation in high-voltage spinel oxides.[165,166]

Generalizing the structural features and degradation mechanisms of a wide range of polyanionic compounds is difficult, but changes in their unit cell volume are usually large (>6%) during delithiation owing to the ionic nature of the TM–O bonds, *i.e.* approximately 7% for high-voltage olivine $Li_{1-x}CoPO_4$.[167] Particularly in the bi-phasic electrode reactions that proceed with phase boundary movement, large mechanical strain arises in the region between lithium-rich and lithium-poor phases, occasionally causing cracks during (de)lithiation (Fig. 5a).[168]

In any cases, an effective way to suppress cation migration and cracks upon cycling is to use dopants that are electrochemically inactive at the expense of the specific capacity in three scenarios: (i) redox-inactive dopants typically suppress over-delithiation at high voltages, (ii) while also disturbing the cooperative behaviors (*e.g.* phase transition) of the delithiated states. In parallel, (iii) heterodoping can modulate the morphology of secondary particles. Scenario (i) should decelerate cation migration, whereas scenarios (ii) and (iii) may relieve mechanical strain at domain boundaries (Fig. 5b). Because the redox-inactive dopants prevent the over-oxidation of oxide ions in lithium-rich layered oxides, the release of O_2 gas can also be suppressed. Indeed, various cations and anions (such as B, F, Mg, and Al) have been investigated as dopants for positive-electrode materials with high energy density, all of which improved capacity retention during charge/discharge cycling.[71–77,92,93,102,103,106–109,169–173] For example, doping B into a nickel-rich layered oxide was reported to increase capacity retention after 100 cycles from 83% to 92% by suppressing crack formation.[92]

4.2. Interfacial degradation

Synergistic degradation occurs at the interface between a positive-electrode material and electrolyte (Fig. 5a). For example, hydrofluoric acid, which is generated by H_2O contamination or anodic dissociation, such as $PF_6^- \leftrightarrow F^\bullet + PF_5 + e^-$, reacts with most positive-electrode materials to generate LiF and TMF_n.[153] Then, TM^{n+} dissolves into the electrolyte and migrates to the negative electrode. Finally, TM^{n+} is reduced and deposits on the negative electrode, where it causes unfavorable catalytic decomposition of the electrolyte and increases the internal resistance of the cell.[174–178] Subsequently, TM dissolution generates active pits on the positive-electrode surface, causing the additional oxidation of the electrolytes.[175] In parallel, oxidized electrolyte solvents have been postulated to accelerate TM dissolution.[180]

Analogously to the solid-electrolyte interphases (SEI) of negative electrodes, the formation of a CEI is a natural way to suppress interfacial degradation *via* TM dissolution. The chemically and electrochemically stable CEI that uniformly forms on positive electrodes is expected to passivate the electrode surface from damaging chemical reagents such as HF.[84,181,182] However, the naive CEI of high-energy-density positive electrodes with conventional carbonate electrolytes cannot effectively protect the electrode surface. Intensive research has revealed the complex components of CEI in high-energy-density positive electrodes, such as Li_2CO_3 (mainly from an initial contaminant), polycarbonates (from oxidation of linear/cyclic carbonates), PO_xF_y (from oxidation of PF_6^-), TMF_n (from HF attack), and LiF (from PF_6^-

dissociation).[169,171,183–185] Importantly, the CEI composition depends on the electrode potential (*i.e.* electrochemically unstable).[40,186,187] In addition, a non-uniform CEI is formed by damage (cracks or pits) on the surface of positive-electrode materials. Meso/macroscopic cracks generate new reactive surfaces that cause parasitic oxidation of electrolytes.[179,188] All these drawbacks associated with naive CEIs make the effective passivation of the positive electrodes difficult, thus calling for technical solutions.

To address the aforementioned interfacial issues, coating positive-electrode materials is a popular approach (Fig. 5b) for (i) suppressing electrophilic attack from an electrode to an electrolyte while allowing ion transfer, (ii) protecting them from damaging chemical reagents such as HF, thus preventing TM from dissolving to the electrolyte, and (iii) forming a rigid shell to restrict crack formation upon cycling. Indeed, several materials, including ionic conductors,[50,51,54,66,67,189] mixed conductors (active materials),[46,56–58,60,190–192] organic compounds,[58,60,193,194] and electrochemically inactive oxides/polyanionic compounds[44,45,47–49,52,53,55,59,61–65,68–70,195–201] have been investigated as coatings for passivating the active surface of large-capacity/high-voltage electrode materials. For example, a B_2O_3-coated nickel-rich layered oxide retained 85% of its capacity after 200 cycles, significantly more than that of a pristine compound (68%).[70]

Another effective approach for the formation of a CEI is to utilize the oxidative decomposition of electrolytes or its additives that contain specific elements, such as boron,[41,78–82,202–207] silicon,[203,206,208–212] phosphorous,[83–86,207,209–211,213–221] sulfur,[87,204,205,211,222–233] and fluorine.[41,78,82,83,85,86,88,89,156,182,188,205,207,213–215,217,219–221,234,235] Additives that are vulnerable to oxidation and contain nucleophilic B, Si, P and S elements are expected to preferentially oxidize to form a uniform CEI at the positive-electrode surface. In the presence of fluorine-containing components or additives, a fluorine-rich, electrochemically stable, ion-conducting surface film forms, composed of complex deposits of Li–X–O/F (X = B, Si, P, and S) that effectively behave as a CEI. The mechanisms underlying its functionality are as follows: (i) $XO_xF_y^{n-}$ scavenges oxidized radicals and hydrofluoric acid, (ii) microporous/amorphous Li–*X*–O/F enables fast Li^+ transfer while (iii) hindering interfacial electron transfer. For instance, when 0.6 M LiTFSI + 0.4 M lithium bis(oxalato)borate (LiBOB) + 0.05 M $LiPF_6$ in ethylene carbonate (EC)/EMC (4 : 6 by weight) was used as an electrolyte for $LiNi_{0.76}Mn_{0.14}Co_{0.1}O_2$, a low impedance CEI comprising ion-conducting/electronic-insulating components (polycarbonates, Li–B–O, and Li_2CO_3) formed that achieved a capacity retention greater than 80% after 1000 cycles.[81]

4.3. Electrode disintegration

Using a functional polymer as a binder also effectively improves the electrochemical properties of large-capacity/high-voltage positive electrodes, as its functional groups, such as carboxyl and hydroxyl groups, scavenge damaging radicals or hydrofluoric acid. In addition, adhesive polymers acting as an artificially deposited uniform CEI could mechanically suppress crack formation and particle disintegration in positive-electrode materials, while simultaneously preventing TM from dissolving into the electrolyte. Typical examples include engineering polymers such as polyimides,[90,91,236–239] commodity polymers such as polyacrylates,[240–242] and semisynthetic polymers such as styrene–butadiene rubber/carboxymethyl cellulose,[242–245] *etc.*[246–249] For example, polyimides possess heterocyclic imide rings that strongly interact with the surface of positive electrodes, thus forming a uniform protective film. These rigid imide rings also provide mechanical strength to composite electrodes for minimizing their disintegration due to the pulverization of the active materials. Using a polyimide as a binder for a NCM811 electrode increased the capacity retention after 100 cycles from 30% to 79%.[90] Furthermore, the fluorination of the polyimide binder improved both oxidation and thermal stability, enabling the stable operation of lithium-rich layered oxide $Li_{1.13}Mn_{0.463}Ni_{0.203}Co_{0.203}O_2$.[240]

5. Technical priority analysis

As positive-electrode materials with high energy density suffer from severe performance degradation arising from both bulk (*i.e.* cation migration and cracking) and interfacial (*i.e.* TM dissolution and non-uniform CEI formation) issues, several technical solutions including doping, coating, electrolyte additives, electrolyte fluorination, and functional binders have been intensively investigated (Fig. 6a), as explained in previous sections. Although each technical solution was demonstrated to improve the electrode performance, hierarchizing their effectiveness is important for prioritizing technical solutions. We applied a machine-learning technique to the reported capacity retentions of large-capacity/high-voltage positive-electrode materials.[38,41,44–112,169–173,189–249] The supervised learning of capacity retention after 50 cycles was conducted using a random forest regression with six simple features, *i.e.* coating, doping, electrolyte additives, functional binders, cut-off voltage, and *C*-rate. Target data (capacity retention) was transformed to its improvement index (the ratio of the capacity retentions with/without coating, doping, electrolyte additives, and functional binders).

Fig. 6b compares the predicted and actual improvements in cycle stability ($R^2 = 0.75$ and 0.52 for the training and test data, respectively), which suggests a relatively high variance in the model due to the limited number of data. However, the prediction model clearly indicates that the use of functional binders is the most effective strategy for improving the capacity retention after 50 cycles (Fig. 6c). Functional binders can form uniform artificial CEIs, which offer multiple functions (HF scavenging, protection from TM dissolution, and mechanical integration of the composite) in retaining the electrode performance. Fig. 6c also indicates that coating does not significantly contribute towards improving the capacity retention, relative to doping and electrolyte additives. Thus, if a coating process is costly, it may not be the first choice for enhancing electrode performance.

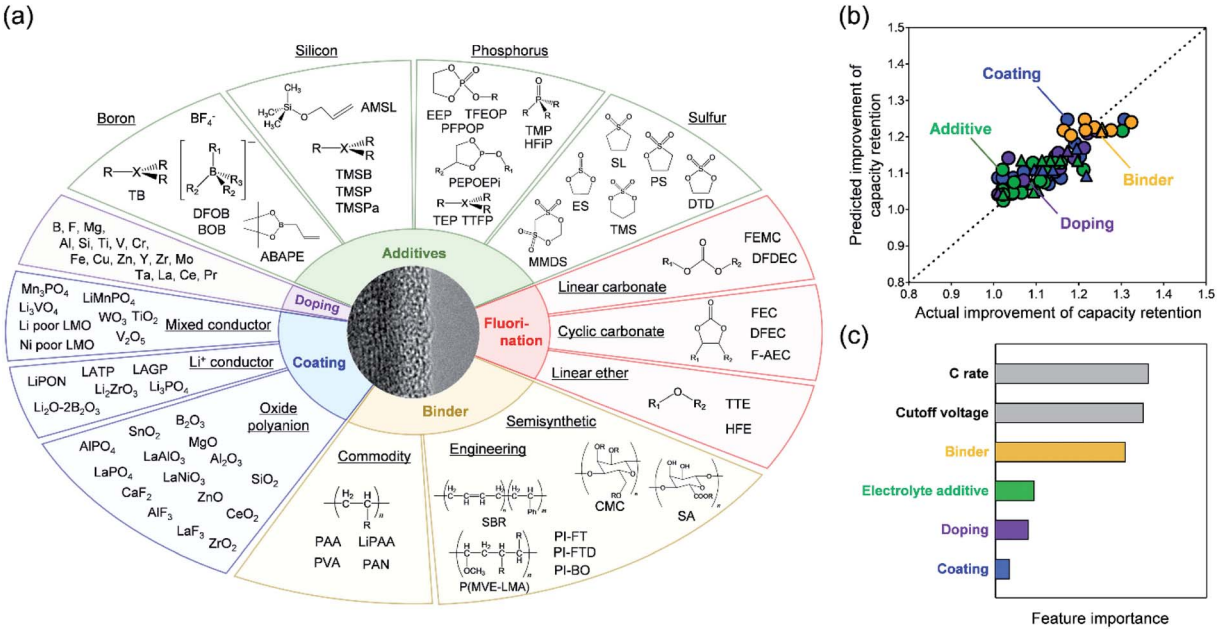

Fig. 6 (a) Previous attempts to improve the performance of large-capacity/high-voltage positive electrodes. (b) Predicted *versus* actual improvements to the capacity retention of large-capacity/high-voltage positive electrodes after 50 cycles. The improvement is the ratio of the capacity retention after 50 cycles with/without coating, doping, additives, and binders. Circles and triangles are the training and test data, respectively. (c) Feature importance in the prediction model from the random forest regression.

6. Summary and perspectives

This review summarizes the issues associated with large-capacity/high-voltage positive-electrode materials for high-energy-density LIBs and their technical solutions. Both a large capacity (large $D(\varepsilon)$ for $\varepsilon_F > \varepsilon > \varepsilon_F - F\Delta E + \Delta\mu_{Li^+}$) and high voltage (low μ_{Li^+} or low μ_{e^-}) are intrinsically prone to accelerating performance degradation in the bulk and at the interface. Several technical solutions have been proposed to address these issues. Electrode materials have been typically doped to resolve bulk issues, whereas electrode coating, electrolyte additives, and functional binders have been used to mitigate interfacial issues. However, the machine-learning analyses of reported data clearly indicate that the use of functional binders is most effective for improving capacity retention, and hence, the further exploration of novel binders that can retain either a large capacity or high voltage should be prioritized.

In addition to the above-mentioned technical solutions, a less explored approach for achieving a longer calendar life is the development of novel large-capacity or high-voltage positive-electrode materials, which possess functionalities that stabilize the electrode during cycling. For example, O2-type layered oxides $LiTMO_2$ and $Li_{1+x}TM_{1-x}O_2$ (O2: lithium ions occupy octahedral sites in a close-packed oxide-ion array of ABCBA) mitigate TM migration due to TM–TM coulombic repulsion, which suppresses capacity fade and voltage decay during cycling.[250–252] In addition, a layered structure self-organizes upon cycling *via* coulombic attractions between ions and vacancies in $Na_{2-x}RuO_3$, which can effectively retain a large capacity.[253,254] Transition-metal vacancies can generate nonbonding O 2p states, leading to a highly reversible and stable oxygen-redox capacity, as reported for $Na_{2-x}Mn_3O_7$.[255] Essentially, precisely controlling the arrangement of transition metals, transition-metal vacancies, and oxide ions could yield novel functionalities that ameliorate the unsatisfactory performance of the present high-energy-density positive electrodes.

As for other important performance such as safety, rate capability, and coulombic efficiency, the amount of reported data is limited; therefore, identifying the most effective technical solution is difficult at this point. For example, the use of functional binders, which most effectively helps in retaining a large capacity, should degrade the rate performance because the artificial CEI of the binders decelerates interfacial ion transfer. However, the trade-off between rate performance degradation and capacity retention is not clearly mentioned in most reports, making systematic data analysis futile. Another consideration missing from this work is that the performance of the positive-electrode materials can be highly susceptible to the counter electrode; the data analysed in this work were only from the results of half cells. In addition, several important features, such as separator, electrolyte composition, and temperature, were not considered. Thus, although the present machine-learning techniques provide a firm proof of concept, they are still not enough to provide an overall protocol for accurate predictions together with hierarchical features behind.

Notably, owing to the limited amount of experimental data, which is far smaller than the usual amount used in 'big data' analyses, it is unrealistic to develop an accurate prediction model with multiple features that fully describe the chemical structures and properties of battery components. For instance, rationally designed fluorinated cyclic phosphate serves as a fire-extinguishing solvent for highly safe electrolytes, as organic

phosphates can trap hydrogen radicals and prevent combustion.[256–259] Although such molecular design is a promising approach for high-energy-density batteries, it is highly challenging to choose informative features from their complex chemical structure and properties for predicting and evaluating additional functionalities. Thus, carefully selecting discriminating features and target functionalities is crucial for reliable data analysis and prediction.

After collecting systematic experimental data, machine learning plays an essential role in data analysis. Indeed, various machine-learning techniques have recently been applied to predict battery performance metrics, *e.g.* voltage, cycle life, and state of charge.[260–266] Once feature importance is identified with hierarchical and quantitative accuracy and reliability, the underlying chemical/physical relationships between electrode performance and several controllable parameters can also be clarified. This comprehensive understanding would enable the rational development of optimal large-capacity/high-voltage positive electrodes.[267]

7. Methods

Electrolytes were prepared by dissolving lithium salts in solvents in an Ar-filled glove box. Lithium bis(fluorosulfonyl) imide (LiFSI) and lithium bis(trifluoromethanesulfonyl)imide (LiTFSI) salts were provided by Nippon Shokubai. Other salts ($LiBF_4$ and $LiPF_6$) and solvents (ethylene carbonate (EC), dimethyl carbonate (DMC), 1,2,-dimethoxyethane (DME), fluoroethylene carbonate (FEC)) were purchased from Kishida Chemicals. $LiMn_2O_4$ was purchased from Hohsen. $LiCoPO_4$ was synthesized using a sol–gel process. Specifically, $LiNO_3$, $Co(NO_3)_2 \cdot 6H_2O$, $NH_4H_2PO_4$, and citric acid were dissolved in distilled water at a molar ratio of 1 : 1 : 1 : 2. The mixture was stirred at 80 °C for 30 min and then dried at 120 °C overnight in an oven. $LiCoPO_4$ was obtained by heating the resultant brown gel at 350 °C for 3 h and then 800 °C for 12 h. For the carbon coating, $LiCoPO_4$ powder was ball-milled with acetylene black (Li400, Denka) in a weight ratio of 9 : 1, followed by heating at 400 °C for 1 h under flowing Ar. All the chemicals were purchased from Wako. For the carbon electrodes, acetylene black and polyvinylidene difluoride (PVdF, Kureha) binder were mixed in *N*-methylpyrrolidone (NMP, Wako) in a weight ratio of 50 : 50. For the $LiMn_2O_4$ and $LiCoPO_4$ electrodes, the active materials, acetylene black, and PVdF binder were mixed in a weight ratio of 80 : 10 : 10 in NMP. The prepared slurries were cast onto Al foil (Fuchikawa Rare Metal) and dried at 80 °C in an oven. The loading level for $LiMn_2O_4$, $LiCoPO_4$, and carbon electrodes were controlled to be 1.8–2.1, 2.9–3.0, and 0.3–0.4 mg cm^{-2}, respectively. The oxidation durability of electrolytes with Al, carbon, $LiMn_2O_4$, and $LiCoPO_4$ electrodes was evaluated *via* linear sweep voltammetry from open circuit potential to 6 V (*vs.* Li/Li^+) at a scan rate of 0.1 mV s^{-1} at 30 °C using VMP3 potentiostat (BioLogic) and 2032-type coin cell with Li metal as the counter electrode.

All the machine learning was conducted using scikit-learn on Python. A random forest regression was selected as the prediction model based on nested cross-validation (*k*-fold cross-validation and grid search for hyperparameter optimization) of several regression models. The determination coefficient (R^2) was calculated as follows:

$$R^2 = 1 - \frac{\sum_{i=1}^{n} (y_i - u_i)^2}{\sum_{i=1}^{n} \left(y_i - \overline{u}_i\right)^2}$$

where y_i, u_i, and $\overline{u_i}$ are the predicted, actual, and averaged values, respectively. The features were simplified to avoid high variance due to the limited amount of data. For example, the chemical information (elements and structures) of the coating, doping, electrolyte additives, and binders was not explicitly considered (one-hot encoding), whereas the electrolyte composition (solvents, anion, and concentration) was ignored in the predictions. The predictions considered both an upper cut-off voltage and charge/discharge *C*-rate.

Conflicts of interest

There are no conflicts to declare.

Acknowledgements

This work was financially supported by the Ministry of Education, Culture, Sports, Science and Technology (MEXT), Japan; Grant-in-Aid for Specially Promoted Research No. 15H05701 and Scientific Research (S) No. 20H05673. M. O. was financially supported by JSPS KAKENHI Grant Numbers 19H05816, 18K19124, 18H03924, and the Asahi Glass Foundation.

References

1 IEA, *Global EV Outlook 2019*, IEA, Paris, 2019, https://www.iea.org/reports/global-ev-outlook-2019.
2 US Advanced Battery Consortium, *USABC Goals for Advanced High-Performance Batteries for Electric Vehicle (EV) Applications*, http://www.uscar.org/guest/article_view.php?articles_id=85.
3 D. Larcher and J. M. Tarascon, *Nat. Chem.*, 2015, **7**, 19–29.
4 X. Zeng, M. Li, D. A. El-Hady, W. Alshitari, A. S. Al-Bogami, J. Lu and K. Amine, *Adv. Energy Mater.*, 2019, **9**, 1900161.
5 K. Mizushima, P. C. Jones, P. J. Wiseman and J. B. Goodenough, *Mater. Res. Bull.*, 1980, **15**, 783–789.
6 M. M. Thackeray, P. J. Johnson, L. A. de Picciotto, P. G. Bruce and J. B. Goodenough, *Mater. Res. Bull.*, 1984, **19**, 179–187.
7 A. K. Padhi, K. S. Nanjundaswamy and J. B. Goodenough, *Journal of the Electrochemical Society*, 1997, **144**, 1188–1194.
8 A. Manthiram, *Nat. Commun.*, 2020, **11**, 1550.
9 M. S. Whittingham, *Chem. Rev.*, 2004, **104**, 4271–4302.
10 C. Masquelier and L. Croguennec, *Chem. Rev.*, 2013, **113**, 6552–6591.
11 A. Yamada, S. C. Chung and K. Hinokuma, *J. Electrochem. Soc.*, 2001, **148**, A224–A229.
12 J. Dahn, U. von Sacken and C. Michal, *Solid State Ionics*, 1990, **44**, 87.

13 Z. Liu, A. Yu and J. Y. Lee, *J. Power Sources*, 1999, **81–82**, 416.
14 F. Schipper, E. M. Erickson, C. Erk, J. Y. Shin, F. F. Chesneau and D. Aurbach, *J. Electrochem. Soc.*, 2017, **164**, A6220–A6228.
15 Z. Lu, D. D. MacNeil and J. Dahn, *ECS Solid State Lett.*, 2001, **4**, A191–A194.
16 Z. Lu and J. Dahn, *J. Electrochem. Soc.*, 2002, **149**, A815–A822.
17 G. Assat and J. M. Tarascon, *Nat. Energy*, 2018, **3**, 373–386.
18 Q. Zhong, A. Bonakdarpour, M. Zhang, Y. Gao and J. R. Dahn, *J. Electrochem. Soc.*, 1997, **144**, 205–213.
19 W. Li, B. Song and A. Manthiram, *Chem. Soc. Rev.*, 2017, **46**, 3006–3059.
20 K. Amine, H. Yasuda and M. Yamachi, *Electrochem. Solid-State Lett.*, 2000, **3**, 178.
21 M. Zhang, N. Garcia-Araez and A. L. Hector, *J. Mater. Chem. A*, 2018, **6**, 14483–14517.
22 A. Chakraborty, S. Kunnikuruvan, S. Kumar, B. Markovsky, D. Aurbach, M. Dixit and D. T. Major, *Chem. Mater.*, 2020, **32**, 915–952.
23 H. H. Sun, H. H. Ryu, U. H. Kim, J. A. Weeks, A. Heller, Y. K. Sun and C. B. Mullins, *ACS Energy Lett.*, 2020, **5**, 1136–1146.
24 H. M. K. Sari and X. Li, *Adv. Energy Mater.*, 2019, **9**, 1901597.
25 E. M. Erickson, F. Schipper, T. R. Penki, J. Y. Shin, C. Erk, F. F. Chesneau, B. Markovsky and D. Aurbach, *J. Electrochem. Soc.*, 2017, **164**, A6341–A6348.
26 P. Rozier and J. M. Tarascon, *J. Electrochem. Soc.*, 2015, **162**, A2490–A2499.
27 S. Hy, H. Liu, M. Zhang, D. Qian, B. J. Hwang and Y. S. Meng, *Energy Environ. Sci.*, 2016, **9**, 1931–1954.
28 H. Xu, H. Zhang, J. Ma, G. Xu, T. Dong, J. Chen and G. Cui, *ACS Energy Lett.*, 2019, **4**, 2871–2886.
29 M. Gauthier, T. J. Carney, A. Grimaud, L. Giordano, N. Pour, H. H. Chang, D. P. Fenning, S. F. Lux, O. Paschos, C. Bauer, F. Maglia, S. Lupart, P. Lamp and Y. Shao-Horn, *J. Phys. Chem. Lett.*, 2015, **6**, 4653–4672.
30 A. M. Haregewoin, A. S. Wotango and B. J. Hwang, *Energy Environ. Sci.*, 2016, **9**, 1955–1988.
31 T. Kim, W. Song, D. Y. Son, L. K. Ono and Y. Qi, *J. Mater. Chem. A*, 2019, **7**, 2942–2964.
32 H. Zhang, H. Zhao, M. A. Khan, W. Zou, J. Xu, L. Zhang and J. Zhang, *J. Mater. Chem. A*, 2018, **6**, 20564–20620.
33 J. Duan, X. Tang, H. Dai, Y. Yang, W. Wu, X. Wei and Y. Huang, *Electrochem. Energy Rev.*, 2020, **3**, 1–42.
34 T. Li, X. Z. Yuan, L. Zhang, D. Song, K. Shi and C. Bock, *Electrochem. Energy Rev.*, 2020, **3**, 43–80.
35 E. Rossen, C. D. W. Jones and J. R. Dahn, *Solid State Ionics*, 1992, **57**, 311–318.
36 T. Ohzuku, A. Ueda, M. Nagayama, Y. Iwakoshi and H. Komori, *Electrochim. Acta*, 1993, **38**, 1159–1167.
37 H. J. Noh, S. Youn, C. S. Yoon and Y. K. Sun, *J. Power Sources*, 2013, **233**, 121–130.
38 H. Q. Pham, E. H. Hwang, Y. G. Kwon and S. W. Song, *Chem. Commun.*, 2019, **55**, 1256–1258.
39 N. Yabuuchi and T. Ohzuku, *J. Power Sources*, 2003, **119–121**, 171–174.
40 J. Zhang, Q. Li, Y. Wang, J. Zheng, X. Yu and H. Li, *Energy Storage Materials*, 2018, **14**, 1–7.
41 T. Deng, X. Fan, L. Cao, J. Chen, S. Hou, X. Ji, L. Chen, S. Li, X. Zhou, E. Hu, D. Su, X. Q. Yang and C. Wang, *Joule*, 2019, **3**, 2550–2564.
42 A. R. Armstrong and P. G. Bruce, *Nature*, 1996, **381**, 499–500.
43 A. Yamada, K. Miura, K. Hinokuma and M. Tanaka, *J. Electrochem. Soc.*, 1995, **142**, 2149–2156.
44 Z. Gan, G. Hu, Z. Peng, Y. Cao, H. Tong and K. Du, *Appl. Surf. Sci.*, 2019, **481**, 1228–1238.
45 Z. Chen, Y. Liu, Z. Lu, R. Hu, J. Cui, H. Xu, Y. Ouyang, Y. Zhang and M. Zhu, *J. Alloys Compd.*, 2019, **803**, 71–79.
46 U. H. Kim, H. H. Ryu, J. H. Kim, R. Mucke, P. Kaghazchi, C. S. Yoon and Y. K. Sun, *Adv. Energy Mater.*, 2019, **9**, 1803902.
47 Y. Xu, X. Li, Z. Wang, H. Guo, W. Peng and W. Pan, *Electrochim. Acta*, 2016, **219**, 49–60.
48 J. Duan, C. Wu, Y. Cao, K. Du, Z. Peng and G. Hu, *Electrochim. Acta*, 2016, **221**, 14–22.
49 W. Cho, S. M. Kim, K. W. Lee, J. H. Song, Y. N. Jo, T. Yim, H. Kim, J. S. Kim and Y. J. Kim, *Electrochim. Acta*, 2016, **198**, 77–83.
50 H. Liang, Z. Wang, H. Guo, J. Wang and J. Leng, *Appl. Surf. Sci.*, 2017, **423**, 1045–1053.
51 M. Wang, R. Zhang, Y. Gong, Y. Su, D. Xiang, L. Chen, Y. Chen, M. Luo and M. Chu, *Solid State Ionics*, 2017, **312**, 53–60.
52 Y. C. Li, W. M. Zhao, W. Xiang, Z. G. Wu, Z. G. Yang, C. L. Xu, Y. D. Xu, E. H. Wang, C. J. Wu and X. D. Guo, *J. Alloys Compd.*, 2018, **766**, 546–555.
53 S. H. Lee, G. J. Park, S. J. Sim, B. S. Jim and H. S. Kim, *J. Alloys Compd.*, 2019, **791**, 193–199.
54 M. Du, P. Yang, W. He, S. Bie, H. Zhao, J. Yin, Z. G. Zou and J. Liu, *J. Alloys Compd.*, 2019, **805**, 991–998.
55 H. Tong, P. Dong, J. Zhang, J. Zheng, W. Yu, K. Wei, B. Zhang, Z. Liu and D. Chu, *J. Alloys Compd.*, 2018, **764**, 44–50.
56 Y. Lee, H. Kim, T. Yim, K. Y. Lee and W. Choi, *J. Power Sources*, 2018, **400**, 87–95.
57 B. Zhang, P. Dong, H. Tong, Y. Yao, J. Zheng, W. Yu, J. Zhang and D. Chu, *J. Alloys Compd.*, 2017, **706**, 198–204.
58 W. Luo and B. Zhang, *Appl. Surf. Sci.*, 2017, **404**, 310–317.
59 L. A. Riley, S. V. Atta, A. S. Cavanagh, Y. Yan, S. M. George, P. Liu, A. C. Dilon and S. H. Lee, *J. Power Sources*, 2011, **196**, 3317–3324.
60 S. Chen, T. He, Y. Su, Y. Lu, L. Bao, L. Chen, Q. Zhang, J. Wang, R. Chen and F. Wu, *ACS Appl. Mater. Interfaces*, 2017, **9**, 29732–29743.
61 D. Becker, M. Borner, R. Nolle, M. Diehl, S. Klein, U. Todehorst, R. Schmuch, M. Winter and T. Placke, *ACS Appl. Mater. Interfaces*, 2019, **11**, 18404–18414.
62 Y. Wu, H. Ming, M. Li, J. Zhang, W. Wahyudi, L. Xie, X. He, J. Wang, Y. Wu and J. Ming, *ACS Energy Lett.*, 2019, **4**, 656–665.

63 Y. Wu, M. Li, W. Wahyudi, G. Sheng, X. Miao, T. D. Anthopoulos, K. W. Huang, Y. Li and Z. Lai, *ACS Omega*, 2019, **4**, 13972–13980.
64 S. W. Lee, M. S. Kim, J. H. Jeong, D. H. Kim, K. Y. Chung, K. C. Roh and K. B. Kim, *J. Power Sources*, 2017, **360**, 206–214.
65 B. C. Park, H. B. Kim, S. T. Myung, K. Amine, I. Belharouak, S. M. Lee and Y. K. Sun, *J. Power Sources*, 2008, **178**, 826–831.
66 Y. S. Park, K. H. Choi, H. K. Park and S. M. Lee, *J. Electrochem. Soc.*, 2010, **157**, A850–A853.
67 G. Song, H. Zhong, Z. Wang, Y. Dai, X. Zhou and J. Yang, *ACS Appl. Energy Mater.*, 2019, **2**, 7923–7932.
68 H. J. Song, S. H. Jiang, J. Ahn, S. H. Oh and T. Yim, *J. Power Sources*, 2019, **416**, 1–8.
69 S. H. Jang, K. J. Lee, J. Mun, Y. K. Han and T. Yim, *J. Power Sources*, 2019, **410–411**, 15–24.
70 Q. Xie, W. Li, A. Dolocan and A. Manthiram, *Chem. Mater.*, 2019, **31**, 8886–8897.
71 Z. Qiu, Z. Liu, X. Fu, J. Liu and Q. Zeng, *J. Alloys Compd.*, 2019, **806**, 136–145.
72 Y. Zhang, T. Ren, J. Zhang, J. Duan, X. Li, Z. Zhou, P. Dong and D. Wang, *J. Alloys Compd.*, 2019, **805**, 1288–1296.
73 H. H. Ryu, N. Y. Park, J. H. Seo, Y. S. Yu, M. Sharma, R. Mucke, P. Kaghazchi, C. S. Yoon and Y. K. Sun, *Mater. Today*, 2020, **36**, 73–82.
74 S. J. Sim, S. H. Lee, B. S. Jin and H. S. Kim, *Sci. Rep.*, 2019, **9**, 8952.
75 A. M. Hashem, A. E. Abdel-Ghany, M. Scheuermann, S. Indris, H. Ehrenberg, A. Mauger and C. M. Julien, *Materials*, 2019, **12**, 2899.
76 C. Lv, J. Yang, Y. Peng, X. Duan, J. Ma, Q. Li and T. Wang, *Electrochim. Acta*, 2019, **297**, 258–266.
77 H. Xu, L. Ai, J. Yan, G. Yan and W. Zhang, *Ceram. Int.*, 2019, **45**, 23089–23096.
78 X. Zuo, C. Fan, J. Liu, X. Xiao, J. Wu and J. Nan, *J. Electrochem. Soc.*, 2013, **160**, A1199–A1204.
79 Z. Wang, L. Xing, J. Li, B. Li, M. Xu, Y. Liao and W. Li, *Electrochim. Acta*, 2015, **184**, 40–46.
80 L. Zhang, Y. Ma, X. Cheng, P. Zuo, Y. Cui, T. Guan, C. Du, Y. Gao and G. Yin, *Solid State Ionics*, 2014, **263**, 146–151.
81 W. Zhao, J. Zheng, L. Zou, H. Jia, B. Liu, H. Wang, M. H. Engelhard, C. Wang, W. Xu, Y. Yang and J. G. Zhang, *Adv. Energy Mater.*, 2018, **8**, 1800297.
82 G. Lan, H. Zhou, L. Xing, J. Chen, Z. Li, R. Guo, Y. Che and W. Li, *J. Energy Chem.*, 2019, **39**, 235–243.
83 C. C. Su, M. He, C. Peebles, L. Zeng, A. Tornheim, C. Liao, L. Zhang, J. Wang, Y. Wang and Z. Zhang, *ACS Appl. Mater. Interfaces*, 2017, **9**, 30686–30695.
84 D. Gao, J. B. Xu, M. Lin, Q. Xu, C. F. Ma and H. F. Xiang, *RSC Adv.*, 2015, **5**, 17566–17571.
85 J. Chen, L. Xing, X. Yang, X. Liu, T. Li and W. Li, *Electrochim. Acta*, 2018, **290**, 568–576.
86 L. Wang, Y. Ma, Q. Li, Y. Cui, P. Wang, X. Cheng, P. Zuo, C. Du, Y. Gao and G. Yin, *Electrochim. Acta*, 2017, **243**, 72–81.
87 P. Dong, D. Wang, Y. Yao, X. Li, Y. Zhang, J. Ru and T. Ren, *J. Power Sources*, 2017, **344**, 111–118.
88 X. Fan, L. Chen, O. Borodin, X. Ji, J. Chen, S. Hou, T. Deng, J. Zheng, C. Yang, S. C. Liou, K. Amine, K. Xu and C. Wang, *Nat. Nanotechnol.*, 2018, **13**, 715–722.
89 Y. M. Lee, K. M. Nam, E. H. Hwang, Y. G. Kwon, D. H. Kang, S. S. Kim and S. W. Song, *J. Phys. Chem. C*, 2014, **118**, 10631–10639.
90 H. Q. Pham, J. Lee, H. M. Jung and S. W. Song, *Electrochim. Acta*, 2019, **317**, 711–721.
91 J. H. Park, J. H. Cho, S. B. Kim, W. S. Kim, S. Y. Lee and S. Y. Lee, *J. Mater. Chem.*, 2012, **22**, 12574–12581.
92 H. H. Ryu, N. Y. Park, D. R. Yoon, U. H. Kim, C. S. Yoon and Y. K. Sun, *Adv. Energy Mater.*, 2020, **10**, 2000495.
93 F. Xin, H. Zhou, X. Chen, M. Zuba, N. Chernova, G. Zhou and M. S. Whittingham, *ACS Appl. Mater. Interfaces*, 2019, **11**, 34889–34894.
94 W. Lee, S. Muhammad, T. Kim, H. Kim, E. Lee, M. Jeong, S. Son, J. H. Ryou and W. S. Yoon, *Adv. Energy Mater.*, 2018, **8**, 1701788.
95 C. H. Jo, D. H. Cho, H. J. Noh, H. Yashiro, Y. K. Sun and S. T. Myung, *Nano Res.*, 2015, **1**, 1464–1479.
96 Z. Cao, M. Hashinokuchi, T. Doi and M. Inaba, *J. Electrochem. Soc.*, 2019, **166**, A82–A88.
97 B. Song, W. Li, S. M. Oh and A. Manthiram, *ACS Appl. Mater. Interfaces*, 2017, **9**, 9718–9725.
98 O. Srur-Lavi, V. Miikkulainen, B. Markovsky, J. Grinblat, M. Talianker, Y. Fleger, G. Cohen-Taguri, A. Mor, Y. Tal-Yosef and D. Aurbach, *J. Electrochem. Soc.*, 2017, **164**, A3266–A3275.
99 K. Meng, Z. Wang, H. Guo, X. Li and D. Wang, *Electrochim. Acta*, 2016, **211**, 822–831.
100 L. Wang, Y. Ma, P. Wang, S. Lou, X. Cheng, P. Zuo, C. Du, Y. Gao and G. Yin, *J. Electrochem. Soc.*, 2017, **164**, A1924–A1932.
101 X. Guo, L. N. Cong, Q. Zhao, L. H. Tai, X. L. Wu, J. P. Zhang, R. S. Wang, H. M. Xie and L. Q. Sun, *J. Alloys Compd.*, 2015, **651**, 12–18.
102 D. Wang, X. Li, Z. Wang, H. Guo, Y. Xu and Y. Fan, *Electrochim. Acta*, 2016, **196**, 101–109.
103 Y. D. Xu, J. Zhang, Z. G. Wu, C. L. Xu, Y. C. Li, W. Xiang, Y. Wang, Y. J. Zhong, X. D. Guo and H. Chen, *Energy Technology*, 2020, **8**, 1900498.
104 S. S. Zhang, J. Chen and C. Wang, *J. Electrochem. Soc.*, 2019, **166**, A487–A492.
105 Y. Li, S. Deng, Y. Chen, J. Gao, J. Zhu, L. Xue, T. Lei, G. Cao, J. Guo and S. Wang, *Electrochim. Acta*, 2019, **300**, 26–35.
106 L. Qiu, W. Xiang, W. Tian, C. L. Xu, Y. C. Li, Z. G. Wu, T. R. Chen, K. Jia, D. Wang D, F. R. He and X. D. Guo, *Nano Energy*, 2019, **63**, 103818.
107 X. Yang, Y. Tang, G. Shang, J. Wu, Y. Lai, J. Li, Y. Qu and Z. Zhang, *ACS Appl. Mater. Interfaces*, 2019, **11**, 32015–32024.
108 F. Schipper, H. Bouzaglo, M. Dixit, E. M. Erickson, T. Weigel, M. Talianker, J. Grinblat, L. Burstein, M. Schmidt, J. Lampert and C. Erk, *Adv. Energy Mater.*, 2018, **8**, 1701682.

109 H. Yang, H. H. Wu, M. Ge, L. Li, Y. Yuan, Q. Yao, J. Chen, L. Xia, J. Zheng, Z. Chen and J. Duan, *Adv. Funct. Mater.*, 2019, **29**, 1808825.
110 A. Yasmin, M. A. Shehzad, J. Wang, X. D. He, X. Ding, S. Wang, Z. Wen and C. Chen, *ACS Appl. Mater. Interfaces*, 2020, **12**, 826–835.
111 R. Zhao, J. Liang, J. Huang, R. Zeng, J. Zhang, H. Chen and G. Shi, *J. Alloys Compd.*, 2017, **724**, 1109–1116.
112 Q. Liu, G. Yang, S. Liu, M. Han, Z. Wang and L. Chen, *ACS Appl. Mater. Interfaces*, 2019, **11**, 17435–17443.
113 M. M. Thackeray, S. H. Kang, C. S. Johnson, J. T. Vaughey, R. Benedek and S. A. Hackney, *J. Mater. Chem.*, 2007, **17**, 3112–3125.
114 S. L. Cui, Y. Y. Wang, S. Liu, G. R. Li and X. P. Gao, *Electrochim. Acta*, 2019, **328**, 135109.
115 K. Luo, M. R. Roberts, N. Guerrini, N. Tapia-Ruiz, R. Hao, F. Massel, D. M. Pickup, S. Ramos, Y. S. Liu, J. Guo, A. V. Chadwick, L. C. Duda and P. G. Bruce, *J. Am. Chem. Soc.*, 2016, **138**, 11211–11218.
116 K. Luo, M. R. Roberts, R. Hao, N. Guerrini, D. M. Pickup, Y. S. Liu, K. Edström, J. H. Guo, A. V. Chadwick, L. C. Duda and P. G. Bruce, *Nat. Chem.*, 2016, **8**, 684–691.
117 D. H. Seo, J. Lee, A. Urban, R. Malik, S. Y. Kang and G. Ceder, *Nat. Chem.*, 2016, **8**, 692–697.
118 M. Okubo and A. Yamada, *ACS Appl. Mater. Interfaces*, 2017, **9**, 36463–36472.
119 E. McCalla, A. M. Abakumov, M. Saubanère, D. Foix, E. J. Berg, G. Rousse, M. L. Doublet, D. Gonbeau, P. Novák, G. Van Tedeloo, R. Dominko and J. M. Tarascon, *Science*, 2015, **350**, 1516–1521.
120 N. Yabuuchi, M. Nakayama, M. Takeuchi, S. Komaba, Y. Hashimoto, T. Mukai, H. Shiiba, K. Sato, Y. Kobayashi, A. Nakao, M. Yonemura, K. Yamanaka, K. Mitsuhara and T. Ohta, *Nat. Commun.*, 2016, **7**, 13814.
121 B. Mortemard de Boisse, S. Nishimura, E. Watanabe, L. Lander, A. Tsuchimoto, J. Kikkawa, E. Kobayashi, D. Asakura, M. Okubo and A. Yamada, *Adv. Energy Mater.*, 2018, **8**, 1800409.
122 J. Hong, W. E. Gent, P. Xiao, K. Lim, D. H. Seo, J. Wu, P. M. Csernia, C. J. Takacs, D. Nordlund, C. J. Sun, K. H. Stone, D. Passerello, W. L. Yang, D. Prendergast, G. Ceder, M. F. Toney and W. C. Chueh, *Nat. Mater.*, 2019, **8**, 256–265.
123 R. A. House, U. Maitra, M. A. Perez-Osorio, J. G. Lozano, L. Jin, J. W. Somerwille, L. C. Dude, A. Nag, A. Walters, K. J. Zhou, M. R. Roberts and P. G. Bruce, *Nature*, 2020, **577**, 502–508.
124 T. Sudayama, K. Uehara, T. Mukai, D. Asakura, X. M. Shi, A. Tsuchimoto, B. Mortemard de Boisse, T. Shimada, E. Watanabe, Y. Harada, M. Nakayama, M. Okubo and A. Yamada, *Energy Environ. Sci.*, 2020, **13**, 1492–1500.
125 H. Koga, L. Croguennec, M. Menetrier, K. Douhil, S. Belin, L. Bourgeois, E. Suard, F. Weil and C. Delmas, *J. Electrochem. Soc.*, 2013, **160**, A786–A792.
126 T. Zheng and J. R. Dahn, *Phys. Rev. B: Condens. Matter Mater. Phys.*, 1997, **56**, 3800–3805.
127 T. Ohzuku, S. Takeda and M. Iwanaga, *J. Power Sources*, 1999, **81–82**, 90–94.
128 C. Sigala, D. Guyomard, A. Verbaere, Y. Piffard and M. Tournoux, *Solid State Ionics*, 1995, **81**, 167–170.
129 H. Kawai, M. Nagata, H. Tukamoto and A. R. West, *J. Mater. Chem.*, 1998, **8**, 837–839.
130 S. Okada, S. Sawa, M. Egashira, J. Yamaki, M. Tabuchi, H. Kageyama, T. Konishi and A. Yoshino, *J. Power Sources*, 2001, **97–98**, 430–432.
131 A. Manthiram and J. B. Goodenough, *J. Power Sources*, 1989, **26**, 403–408.
132 F. Zhou, M. Cococcioni, C. A. Marianetti, D. Morgan and G. Ceder, *Phys. Rev. B: Condens. Matter Mater. Phys.*, 2004, **70**, 235121.
133 F. Zhou, M. Cococcioni, K. Kang and G. Ceder, *Electrochem. Commun.*, 2004, **6**, 1144–1148.
134 M. Herklotz, F. Scheiba, R. Glaum, E. Mosymow, S. Oswald, J. Eckert and H. Ehrenberg, *Electrochim. Acta*, 2014, **139**, 356–364.
135 K. Kawai, W. Zhao, S. Nishimura and A. Yamada, *ACS Appl. Energy Mater.*, 2018, **1**, 928–931.
136 J. Zhang, Y. C. Liu, X. D. Zhao, L. H. He, H. Liu, Y. Z. Song, S. D. Sun, Q. Li, X. R. Xing and J. Chen, *Adv. Mater.*, 2020, **32**, 1906348.
137 K. Kawai, D. Asakura, S. Nishimura and A. Yamada, *Chem. Commun.*, 2019, **44**, 13717–13720.
138 S. Okada, M. Ueno, Y. Uebou and J. Yamaki, *J. Power Sources*, 2005, **146**, 565–569.
139 S. C. Yin, P. Subramanya Herle, A. Higgins, N. J. Taylor, Y. Makimura and L. F. Nazar, *Chem. Mater.*, 2006, **18**, 1745–1752.
140 J. Baker, M. Y. Saidi and J. L. Swoyer, *J. Electrochem. Soc.*, 2003, **150**, A1394–A1398.
141 T. Mueller, G. Hautier, A. Jain and G. Ceder, *Chem. Mater.*, 2011, **23**, 3854–3862.
142 B. L. Ellis, R. M. Makahnouk, Y. Makiura, K. Toghill and L. F. Nazar, *Nat. Mater.*, 2007, **6**, 749–753.
143 N. Recham, J. N. Chotard, L. Dupont, C. Delacourt, W. Walker, M. Armand and J. M. Tarascon, *Nat. Mater.*, 2010, **9**, 68–74.
144 S. Tan, Y. J. Ji, Z. R. Zhang and Y. Yang, *ChemPhysChem*, 2014, **15**, 1956–1969.
145 L. J. Krause, W. Lamanna, J. Summerfield, M. Engle, G. Korba, R. Loch and R. Atanasoski, *J. Power Sources*, 1997, **68**, 320–325.
146 H. Yang, K. Kwon, T. M. Devine and J. W. Evans, *J. Electrochem. Soc.*, 2000, **147**, 4399–4407.
147 Y. Yamada, C. H. Chiang, K. Sodeyama, J. Wang, Y. Tateyama and A. Yamada, *ChemElectroChem*, 2015, **2**, 1687–1694.
148 M. Ue, M. Takeda, M. Takehara and S. Mori, *J. Electrochem. Soc.*, 1997, **144**, 2684–2688.
149 J. M. Tarascon and D. Guyomard, *Solid State Ionics*, 1994, **69**, 293–305.
150 K. Kanamura, T. Okagawa and Z. Takehara, *J. Power Sources*, 1995, **57**, 119.

151 S. Ko, Y. Yamada, L. Lander and A. Yamada, *Carbon*, 2020, **158**, 766–771.
152 Y. Zhang, Y. Katayama, R. Tatara, L. Giordano, Y. Yu, D. Fraggedakis, J. G. Sun, F. Maglia, R. Jung, M. Z. Bazant and Y. Shao-Horn, *Energy Environ. Sci.*, 2020, **13**, 183–199.
153 O. Borodin, W. Behl and T. R. Jow, *J. Phys. Chem. C*, 2013, **117**, 8661–8682.
154 V. R. Koch, *J. Electrochem. Soc.*, 1979, **126**, 181.
155 K. Xu, S. P. Ding and T. R. Jow, *J. Electrochem. Soc.*, 1999, **146**, 4172–4178.
156 Z. Zhang, L. Hu, H. Wu, W. Wang, M. Koh, P. C. Redfern, L. A. Curtiss and K. Amine, *Energy Environ. Sci.*, 2013, **6**, 1806–1810.
157 H. Wang, Y. I. Jang, B. Huang, D. R. Sadoway and Y. M. Chiang, *J. Electrochem. Soc.*, 1999, **146**, 473–480.
158 C. Pouillerie, L. Croguennec and C. Delmas, *Solid State Ionics*, 2000, **132**, 15–29.
159 R. V. Chebiam, F. Prado and A. Manthiram, *J. Electrochem. Soc.*, 2001, **148**, A49–A53.
160 S. Choi and A. Manthiram, *J. Electrochem. Soc.*, 2002, **149**, A1157–A1163.
161 H. H. Ryu, K. J. Park, C. S. Yoon and Y. K. Sun, *Chem. Mater.*, 2018, **30**, 1155–1163.
162 M. Sathiya, G. Rousse, K. Ramesha, C. P. Laisa, H. Vezin, M. T. Sougrati, M. L. Doublet, D. Foix, D. Gonbeau, W. Walker, A. S. Prakash, M. Ben Hassine, L. Dupont and J. M. Tarascon, *Nat. Mater.*, 2013, **12**, 827–835.
163 P. Yan, J. Zheng, Z. K. Tang, A. Devaraj, G. Chen, K. Amine, J. G. Zhang, L. M. Liu and C. Wang, *Nat. Nanotechnol.*, 2019, **14**, 602–608.
164 R. Alcantara, M. Jaraba, P. Lavela and J. L. Tirado, *Electrochim. Acta*, 2002, **47**, 1829–1835.
165 J. H. Kim, C. S. Yoon, S. T. Myung, J. Prakash and Y. K. Sun, *Electrochem. Solid-State Lett.*, 2004, **7**, A216–A220.
166 Y. Gong, Y. Chen, Q. Zhang, F. Meng, J. A. Shi, X. Liu, X. Liu, J. Zhang, H. Wang, J. Wang, Q. Yu, Z. Zhang, Q. Xu, R. Xiao, Y. S. Hu, L. Gu, H. Li, X. Huang and L. Chen, *Nat. Commun.*, 2018, **9**, 3341.
167 N. N. Bramnik, K. Nikolowski, C. Baehtz, K. G. Bramnik and H. Ehrenberg, *Chem. Mater.*, 2007, **19**, 908–915.
168 J. Wolfenstine, B. Poese and J. Allen, *J. Power Sources*, 2004, **138**, 281–282.
169 S. Yamamoto, H. Noguchi and W. Zhao, *J. Power Sources*, 2015, **278**, 76–86.
170 W. Zhao, L. Xiong, Y. Xu, X. Xiao, J. Wang and Z. Ren, *J. Power Sources*, 2016, **330**, 37–44.
171 T. Weigel, F. Schipper, E. M. Erickson, F. A. Susai, B. Markovsky and D. Aurbach, *ACS Energy Lett.*, 2019, **4**, 508–516.
172 F. A. Susai, D. Kovacheva, A. Chakraborty, T. Kravchuk, R. Ravikumar, M. Talianker, J. Grinblat, L. Burstein, Y. Kauffmann, D. T. Major, B. Markovsky and D. Aurbach, *ACS Appl. Energy Mater.*, 2019, **2**, 4521–4534.
173 F. Nobili, F. Croce, R. Tossici, I. Meschini, P. Reale and R. Marassi, *J. Power Sources*, 2012, **197**, 276–284.
174 D. Aurbach, *J. Power Sources*, 2000, **89**, 206–218.
175 D. Aurbach, B. Markovsky, G. Salitra, E. Markevich, Y. Talyossef, M. Koltypin, L. Nazar, B. Ellis and D. Kovacheva, *J. Power Sources*, 2007, **165**, 491–499.
176 W. Li, A. Dolocan, P. Oh, H. Celio, S. Park, J. Cho and A. Manthiram, *Nat. Commun.*, 2018, **8**, 14589.
177 J. Li and A. Manthiram, *Adv. Energy Mater.*, 2019, **9**, 1902731.
178 Y. K. Sun, K. J. Hong, J. Prakash and K. Amine, *Electrochem. Commun.*, 2002, **4**, 344–348.
179 J. Zheng, M. Gu, J. Xiao, B. J. Polzin, P. Yan, X. Chen, C. Wang and J. G. Zhang, *Chem. Mater.*, 2014, **26**, 6320–6327.
180 D. H. Jang, Y. J. Shin and S. M. Oh, *J. Electrochem. Soc.*, 1996, **143**, 2204–2211.
181 S. Jiao, X. Ren, R. Cao, M. H. Engelhard, Y. Liu, D. Hu, D. Mei, J. Zheng, W. Zhao, Q. Li, N. Liu, B. D. Adams, C. Ma, J. Liu, J. G. Zhang and W. Xu, *Nat. Energy*, 2018, **3**, 739–746.
182 D. Sun, Q. Wang, J. Zhou, Y. Lyu, Y. Liu and B. Guo, *J. Electrochem. Soc.*, 2018, **165**, A2032–A2036.
183 K. Edstrom, T. Gustafsson and J. O. Thomas, *Electrochim. Acta*, 2004, **50**, 397–403.
184 D. Chen, M. A. Mahmoud, J. H. Wang, G. H. Waller, B. Zhao, C. Qu, M. A. El-Sayed and M. Liu, *Nano Lett.*, 2019, **19**, 2037–2043.
185 H. Duncan, Y. Abu-Lebdeh and I. J. Davidson, *J. Electrochem. Soc.*, 2010, **157**, A528–A535.
186 Z. W. Lebens-Higgins, S. Sallis, N. V. Faenza, F. Badway, N. Pereira, D. M. Halat, M. Wahila, C. Schlueter, T. L. Lee, W. Yang, C. P. Grey, G. G. Amatucci and L. F. Piper, *Chem. Mater.*, 2018, **30**, 958–969.
187 S. Liu, L. Wang, C. Zhang, B. Chu, C. Wang, T. Huang and A. Yu, *J. Power Sources*, 2019, **438**, 226979.
188 X. Ren, L. Zou, X. Cao, M. H. Engelhard, W. Liu, S. D. Burton, H. Lee, C. Niu, B. E. Matthews, Z. Zhu, C. Wang, B. W. Arey, J. Xiao, J. Liu, J. G. Zhang and W. Xu, *Joule*, 2019, **3**, 1662–1676.
189 W. Liu, P. Oh, X. Liu, S. Myeong, W. Cho and J. Cho, *Adv. Energy Mater.*, 2015, **5**, 1500274.
190 X. Ding, D. Luo, J. Cui, H. Xie, Q. Ren and Z. Lin, *Angew. Chem., Int. Ed.*, 2020, **132**, 7852–7856.
191 Y. K. Sun, S. T. Myung, B. C. Park, J. Prakash, I. Belharouak and K. Amine, *Nat. Mater.*, 2009, **8**, 320–324.
192 Z. Zhu, D. Yu, Y. Yang, C. Su, Y. Huang, Y. Dong, I. Waluyo, B. Wang, A. Hunt, X. Yao, J. Lee, W. Xue and J. Li, *Nat. Energy*, 2019, **4**, 1049–1058.
193 J. Z. Kong, L. P. Xu, C. L. Wang, Y. X. Jiang, Y. Q. Cao and F. Zhou, *J. Alloys Compd.*, 2017, **719**, 401–410.
194 P. Oh, M. Ko, S. Myeong, Y. Kim and J. Cho, *Adv. Energy Mater.*, 2014, **4**, 1400631.
195 M. Si, D. Wang, R. Zhao, D. Pan, C. Zhang, C. Yu, X. Lu, H. Zhao and Y. Bai, *Adv. Sci.*, 2019, 1902538.
196 G. Xu, J. Li, Q. Xue, Y. Dai, H. Zhou, X. Wang and F. Kang, *Electrochim. Acta*, 2014, **117**, 41–47.
197 F. Wu, Q. Li, L. Bao, Y. Zheng, Y. Lu, Y. Su, J. Wang, S. Chen, R. Chen and J. Tian, *Electrochim. Acta*, 2018, **260**, 986–993.

198 K. Park, J. H. Park, B. Choi, J. H. Kim, S. G. Hong and H. N. Han, *Electrochim. Acta*, 2017, **257**, 217–223.
199 K. A. Walz, C. S. Johnson, J. Genthe, L. C. Stoiber, W. A. Zeltner, M. A. Anderson and M. M. Thackeray, *J. Power Sources*, 2010, **195**, 4943–4951.
200 D. Chen, F. Zheng, L. Li, M. Chen, X. Zhong, W. Li and L. Lu, *J. Power Sources*, 2017, **341**, 147–155.
201 M. Bettge, Y. Li, B. Sankaran, N. D. Rago, T. Spila, R. T. Haasch, I. Petrov and D. P. Abraham, *J. Power Sources*, 2013, **233**, 346–357.
202 Z. Luo, H. Zhang, L. Yu, D. Huang and J. Shen, *J. Electroanal. Chem.*, 2019, **833**, 520–526.
203 J. Li, L. Xing, R. Zhang, M. Chen, Z. Wang, M. Xu and W. Li, *J. Power Sources*, 2015, **285**, 360–366.
204 H. Zhou, D. Xiao, C. Yin, Z. Yang, K. Xiao and J. Li, *J. Electroanal. Chem.*, 2018, **808**, 293–302.
205 L. Dong, F. Liang, D. Wang, C. Zhu, J. Liu, D. Gui and C. Li, *Electrochim. Acta*, 2018, **270**, 426–433.
206 Y. Meng, G. Chen, L. Shi, H. Liu and D. Zhang, *ACS Appl. Mater. Interfaces*, 2019, **11**, 45108–45117.
207 B. Liu, H. Zhou, C. Yin, H. Guan and J. Li, *Electrochim. Acta*, 2019, **321**, 134690.
208 J. Chen, H. Zhang, M. Wang, J. Liu, C. Li and P. Zhang, *J. Power Sources*, 2016, **303**, 41–48.
209 Y. K. Han, J. Yoo and T. Yim, *Electrochim. Acta*, 2016, **215**, 455–465.
210 H. Rong, M. Xu, B. Xie, W. Huang, X. Liao, L. Xing and W. Li, *J. Power Sources*, 2015, **274**, 1155–1161.
211 L. Ma, J. Xia and J. R. Dahn, *J. Electrochem. Soc.*, 2015, **162**, A1170–A1174.
212 K. Kim, D. Hwang, S. Kim, S. O. Park, H. Cha, Y. S. Lee, J. Cho, S. K. Kwak and N. S. Choi, *Adv. Energy Mater.*, 2020, 2000012.
213 M. Xu, Y. Liu, B. Li, W. Li, X. Li and S. Hu, *Electrochem. Commun.*, 2012, **18**, 123–126.
214 J. Pires, A. Castets, L. Timperman, J. Santos-Pena, E. Dumont, S. Levasseur, C. Tessier, R. Dedryvere and M. Anouti, *J. Power Sources*, 2015, **296**, 413–425.
215 J. Liu, X. Song, L. Zhou, S. Wang, W. Song, W. Liu, H. Long, L. Zhou, H. Wu, C. Feng and Z. Guo, *Nano Energy*, 2018, **46**, 404–414.
216 N. N. Sinha, J. C. Burns and J. R. Dahn, *J. Electrochem. Soc.*, 2014, **161**, A1084–A1089.
217 M. He, C. C. Su, C. Peebles, Z. Feng, J. G. Connell, C. Liao, Y. Wang, I. A. Shkrob and Z. Zhang, *ACS Appl. Mater. Interfaces*, 2016, **8**, 11450–11458.
218 Z. D. Li, Y. C. Zhang, H. F. Xiang, X. M. Ma, Q. F. Yuan, Q. S. Wang and C. H. Chen, *J. Power Sources*, 2013, **240**, 471–475.
219 A. von Cresce and K. Xu, *J. Electrochem. Soc.*, 2011, **158**, A337–A342.
220 S. Tan, Z. Zhang, Y. Li, Y. Li, J. Zhang, Z. Zhou and Y. Yang, *J. Electrochem. Soc.*, 2013, **160**, A285–A292.
221 N. von Aspern, D. Diddens, T. Kobayashi, M. Borner, O. Stubbmann-Kazakova, V. Kozel, G. V. Roschenthaler, J. Smiatek, M. Winter and I. Cekic-Laskovic, *ACS Appl. Mater. Interfaces*, 2019, **11**, 16605–16618.
222 X. Zuo, C. Fan, X. Xiao, J. Liu and J. Nan, *J. Power Sources*, 2012, **219**, 94–99.
223 X. Cui, H. Zhang, S. Li, Y. Zhao, L. Mao, W. Zhao, Y. Li and X. Ye, *J. Power Sources*, 2013, **240**, 476–485.
224 T. Zhang, I. de Meatza, X. Qi and E. Paillard, *J. Power Sources*, 2017, **356**, 97–102.
225 J. Alvarado, M. A. Schroeder, M. Zhang, O. Borodin, E. Gobrogge, M. Olguin, M. S. Ding, M. Gobet, S. Greenbaum, Y. S. Meng and K. Xu, *Mater. Today*, 2018, **21**, 341–353.
226 X. Zheng, T. Huang, G. Fang, Y. Pan, Q. Li and M. Wu, *ACS Appl. Mater. Interfaces*, 2019, **11**, 36244–36251.
227 R. Wang, X. Li, Z. Wang, H. Guo and J. Wang, *Electrochim. Acta*, 2015, **180**, 815–823.
228 L. Madec, J. Xia, R. Petibon, K. J. Nelson, J. P. Sun, I. G. Hill and J. R. Dahn, *J. Phys. Chem. C*, 2014, **118**, 29608–29622.
229 P. Janssen, R. Schmitz, R. Muller, P. Isken, A. Lex-Balducci, C. Schreiner, M. Winter, I. Cekic-Laskovic and R. Schmitz, *Electrochim. Acta*, 2014, **125**, 101–106.
230 J. Xia, J. E. Harlow, R. Petibon, J. C. Burns, L. P. Chen and J. R. Dahn, *J. Electrochem. Soc.*, 2014, **161**, A547–A553.
231 L. Madec, R. Petibon, K. Tasaki, J. Xia, J. P. Sun, I. G. Hill and J. R. Dahn, *Phys. Chem. Chem. Phys.*, 2015, **17**, 27062–27076.
232 J. Xia, N. N. Sinha, L. P. Chen, G. Y. Kim, D. J. Xiong and J. R. Dahn, *J. Electrochem. Soc.*, 2014, **161**, A84–A88.
233 M. H. Park, Y. S. Lee, H. Lee and Y. K. Han, *J. Power Sources*, 2011, **196**, 5109–5114.
234 M. C. Smart, B. V. Ratnakumar, V. S. Ryan-Mowrey, S. Surampudi, G. K. S. Prakash, J. Hu and I. Cheung, *J. Power Sources*, 2003, **119–121**, 359–367.
235 M. Hekmatfar, I. Hasa, R. Eghbal, D. V. Carvalho, A. Moretti and S. Passerini, *Adv. Mater. Interfaces*, 2019, 1901500.
236 H. Q. Pham, G. Kim, H. M. Jung and S. W. Song, *Adv. Funct. Mater.*, 2018, **28**, 1704690.
237 J. H. Cho, J. H. Park, M. H. Lee, H. K. Song and S. Y. Lee, *Energy Environ. Sci.*, 2012, **5**, 7124–7131.
238 G. Qian, L. Wang, Y. Shang, X. He, S. Tang, M. Liu, T. W. Li, G. Zhang and J. Wang, *Electrochim. Acta*, 2016, **187**, 113–118.
239 J. Zhang, Q. Lu, J. Fang, J. Wang, J. Yang and Y. NuLi, *ACS Appl. Mater. Interfaces*, 2014, **6**, 17965–17973.
240 N. P. W. Pieczonka, V. Borgel, B. Ziv, N. Leifer, V. Dargel, D. Aurbach, J. H. Kim, Z. Liu, X. Huang, S. A. Krachkovskiy, G. R. Goward, I. Halalay, B. R. Powell and A. Manthiram, *Adv. Energy Mater.*, 2015, **5**, 1501008.
241 J. Yang, P. Li, F. Zhong, X. Feng, W. Chen, X. Ai, H. Yang, D. Xia and Y. Cao, *Adv. Energy Mater.*, 2020, 1904264.
242 S. Hitomi, K. Kubota, T. Horiba, K. Hida, T. Matsuyama, H. Oji, S. Yasuno and S. Komaba, *ChemElectroChem*, 2019, **6**, 5070–5079.
243 Z. Han, H. Zhan and Y. Zhou, *Mater. Lett.*, 2014, **114**, 48–51.
244 S. Zhang, H. Gu, H. Pan, S. Yang, W. Du, X. Li, M. Gao, Y. Liu, M. Zhu, L. Ouyang, D. Jian and F. Pan, *Adv. Energy Mater.*, 2017, **7**, 1601066.
245 N. Yabuuchi, Y. Kinoshita, K. Misaki, T. Matsuyama and S. Komaba, *J. Electrochem. Soc.*, 2015, **162**, A538–A544.

246 T. Dong, H. Zhang, Y. Ma, J. Zhang, X. Du, C. Lu, X. Shangguan, J. Li, M. Zhang, J. Yang, X. Zhou and G. Cui, *J. Mater. Chem. A*, 2019, **7**, 24594–24601.
247 T. Zhang, J. T. Li, J. Liu, Y. P. Deng, Z. G. Wu, Z. W. Yin, D. Guo, L. Huang and S. G. Sun, *Chem. Commun.*, 2016, **52**, 4683.
248 F. Wu, W. Li, L. Chen, Y. Lu, Y. Su, W. Bao, J. Wang, S. Chen and L. Bao, *J. Power Sources*, 2017, **359**, 226–233.
249 P. P. Prosini, M. Carewska and A. Masci, *Solid State Ionics*, 2015, **274**, 88–93.
250 B. Mortemard de Boisse, J. Jang, M. Okubo and A. Yamada, *J. Electrochem. Soc.*, 2018, **165**, A3630–A3633.
251 D. Eum, B. Kim, S. J. Kim, H. Park, J. Wu, S. P. Cho, G. Yoon, M. H. Lee, S. K. Jung, W. Yang, W. M. Seong, K. Ku, O. Tamwattana, S. K. Park, I. Hwang and K. Kang, *Nat. Mater.*, 2020, **19**, 419–427.
252 C. Cui, X. Fan, X. Zhou, J. Chen, Q. Wang, L. Ma, C. Yang, E. Hu, X. Q. Yang and C. Wang, *J. Am. Chem. Soc.*, 2020, **142**, 8918–8927.
253 B. Mortemard de Boisse, M. Reynaud, J. Ma, J. Kikkawa, S. Nishimura, M. Casas-Cabanas, C. Delmas, M. Okubo and A. Yamada, *Nat. Commun.*, 2019, **10**, 2185.
254 B. Mortemard de Boisse, G. Liu, J. Ma, S. Nishimura, S. C. Chung, H. Kiuchi, Y. Harada, J. Kikkawa, Y. Kobayashi, M. Okubo and A. Yamada, *Nat. Commun.*, 2016, **7**, 11397.
255 B. Mortemard de Boisse, S. Nishimura, E. Watanabe, L. Lander, A. Tsuchimoto, J. Kikkawa, E. Kobayashi, D. Asakura, M. Okubo and A. Yamada, *Adv. Energy Mater.*, 2018, **8**, 1800409.
256 Q. Zheng, Y. Yamada, R. Shang, S. Ko, Y. Y. Lee, K. Kim, E. Nakamura and A. Yamada, *Nat. Energy*, 2020, **5**, 291–298.
257 N. von Aspern, D. Diddens, T. Kobayashi, M. Borner, O. Stubbmann-Kazakova, V. Kozel, G. V. Roschenthaler, J. Smiatek, M. Winter and I. Cekic-Laskovic, *ACS Appl. Mater. Interfaces*, 2019, **11**, 16605.
258 C. C. Su, M. He, C. Peebles, L. Zeng, A. Tornheim, C. Liao, L. Zhang, J. Wang, Y. Wang and Z. Zhang, *ACS Appl. Mater. Interfaces*, 2017, **9**, 30686–30695.
259 J. Wang, Y. Yamada, K. Sodeyama, E. Watanabe, K. Takada, Y. Tateyama and A. Yamada, *Nat. Energy*, 2018, **3**, 22–29.
260 C. Chen, Y. Zuo, W. Ye, X. Li, Z. Deng and S. P. Ong, *Adv. Energy Mater.*, 2020, **10**, 1903242.
261 Z. Jiang, J. Li, Y. Yang, L. Mu, C. Wei, X. Yu, P. Pianetta, K. Zhao, P. Cloetens, F. Lin and Y. Liu, *Nat. Commun.*, 2020, **11**, 2310.
262 N. Kireeva and V. S. Pervov, *Batteries Supercaps*, 2020, **3**, 427–438.
263 A. Killic, Ç. Odabasi, R. Yildirim and D. Eroglu, *Chem. Eng. J.*, 2020, **390**, 124117.
264 R. P. Joshi, J. Eickholt, L. Li, M. Fornari, V. Barone and J. E. Peralta, *ACS Appl. Mater. Interfaces*, 2019, **11**, 18494–18503.
265 K. A. Severson, P. M. Attia, N. Jin, N. Perkins, B. Jiang, Z. Yang, M. H. Chen, M. Aykol, P. K. Herring, D. Fraggedakis, M. Z. Bazant, S. J. Harris, W. C. Chueh and R. D. Braatz, *Nat. Energy*, 2019, **4**, 383–391.
266 A. D. Sendek, E. D. Cubuk, E. R. Antoniuk, G. Cheon, Y. Cui and E. J. Reed, *Chem. Mater.*, 2019, **31**, 342–352.
267 S. Ko, Y. Yamada and A. Yamada, *Batteries Supercaps*, 2020, **3**, 910–916.